Dynamical Stereochemistry on Several Electronic States: A Computational Study of Na* + H_2

M. Ben-Nun,[†,‡] T. J. Martínez,*[,‡] and R. D. Levine[§]

Department of Chemistry and Biochemistry, University of California San Diego, La Jolla, California 92093-0339, Department of Chemistry, University of Illinois, Urbana, Illinois 61801, and The Fritz Haber Research Center for Molecular Dynamics, The Hebrew University, Jerusalem 91904, Israel, and Department of Chemistry and Biochemistry, University of California Los Angeles, Los Angeles, California 90095-1569

Received: March 25, 1997; In Final Form: June 10, 1997[⊗]

The orbital control of stereochemistry is discussed with special reference to the Na (3p ^{2}P) + H_2 collision. As seen by H_2, the p orbital of the electronically excited Na atom is like a quadrupole, which may or may not lock along the molecular axis. Quantum mechanically, variations in the alignment of the orbital represent changes in the electronic state of the system and so dynamical methods which allow for such interstate transitions must be used. A new, time dependent quantum mechanical method for propagating the wave function on several electronic states is used to study these interstate transitions. Particular attention is given to the question of orbital following. The computational method is fully quantum mechanical but it uses a basis set which takes full account of the classical motion on any given electronic state while the solution of the Schrödinger equation addresses the electronic-state-changing transitions. We pay specific attention to the orbital alignment for both cold and rotationally warm H_2 and for low and high impact parameters throughout the course of the collision. It is concluded that orbital locking is not necessarily instantaneous and can lag behind the faster nuclear motion, including the (fast) rotational motion of H_2.

1. Introduction

Steric effects arise because of the nonspherical charge distribution of the reactants. During the collision this distribution can respond in an adiabatic fashion to the relative motion of the reactants in which case the charge redistribution is continuous and the collision proceeds on a single electronic state. However, the very redistribution of charge, which is inevitable when bonds are broken or formed, means that more than one electronic state is *potentially* involved. The word potentially is in italics because, as we said above, the charge redistribution can be, and often is, an adiabatic change. That is, the electrons continuously and instantly readjust to the motion of the nuclei. Yet, the very need for a charge reorganization contains the potentiality for electronically nonadiabatic effects. Even such a well-studied system as the H + H_2 collision, which in the collinear configuration is almost perfectly electronically adiabatic, has a (high energy) configuration, an equilateral triangle, where a conical intersection[1,2] of the ground and excited states is possible. The effects of this intersection have been the subject of many recent reports, both at this meeting (Stereodynamics of Chemical Reactions)[3] and elsewhere.[4−9]

A particular aspect of charge redistribution is the realignment of orbitals, which, since the pioneering work of Woodward and Hoffmann,[10] has received much attention. In particular, the "orbital following" model of Hertel et al.[11,12] and Rettner and Zare[13] is an example of a potentially nonadiabatic process. The model begins with a (say, laser excited atomic) orbital which is aligned in the laboratory system of coordinates. As the collision begins, this orbital locks in the molecular (body-fixed) system of coordinates and tracks the rotation of this system during the collision. In the molecular (body-fixed) system of coordinates, an atomic orbital which is aligned in the space fixed system is represented as a linear combination of orbitals, a combination determined by the rotation of the molecule fixed frame relative to the laboratory. This coherent combination of orbitals may evolve adiabatically so that the atomic orbital exits from the collision just as it came in. But if, as in our Na* + H_2 example, the molecular frame orbitals give rise to quite different electronic states, there can be state changing transitions.

An analogy to molecular state alignment may be useful. The usual situation is that electrons move more rapidly than atoms. This is the very opposite to molecular rotation, which is often slower than the translation so one is often in the sudden regime. Therefore, if one aligns a molecule, it will often (but not always[14−17]) fail to rotate and lock with respect to its collision partner. With electrons, the opposite is the case. The orbital can lock and follow the rotation of the H_2 molecular axis. What we will discuss below is the possible failure of the electronic locking due to nonadiabatic transitions.

The computational example is a Na (3p ^{2}P) + H_2 collision.[18−31] In particular, Hertel et al.[12] have discussed intuitive models and suitable systems of coordinates for this collision. As seen by H_2, the p orbital of the electronically excited Na atom is like a quadrupole, which may or may not lock along the molecular axis.[16,32−36] In addition, and like H + H_2, this system has a conical intersection determined by symmetry to be at a C_{2v} configuration, where the excited state and the ground state cross. Because one starts with an electronically excited Na atom, this intersection is accessible to thermal reactants. Therefore the Na (3p ^{2}P) + H_2 collision can be used to study two distinct electronically nonadiabatic aspects of charge redistribution: the deformation of shape (i.e., the quenching process, Na (3p ^{2}P) → Na (3s ^{2}S)) and the realignment of the three 3p orbitals. We have already discussed some aspects of the quenching[37,38] and will here emphasize the question of orbital following. The

[†] University of California San Diego.
[‡] University of Illinois.
[§] The Hebrew University and University of California Los Angeles.
[⊗] Abstract published in *Advance ACS Abstracts,* September 15, 1997.

S1089-5639(97)01058-X CCC: $14.00

quantum mechanical procedure that we use is briefly discussed in section 2. It has recently been presented in detail[38−41] and we refer the reader to these papers.

2. Methodology

The essence of the method we use is based on the form

$$\Psi = \sum_I C_I(t)\phi_I(\mathbf{r}_e;\mathbf{R})\chi_I(\mathbf{R};t) \qquad (2.1)$$

for the time dependent total wave function. (Throughout this paper bold letters are used to denote vectors.) Here I is an index of the electronic state and $\phi_I(\mathbf{r}_e;\mathbf{R})$ is the corresponding electronic wave function which can depend parametrically on the set of nuclear coordinates $\mathbf{R}$. The electronic states can be either diabatic or adiabatic, and we use the diabatic representation in this paper. The multidimensional nuclear wave function $\chi_I(\mathbf{R};t)$ is time dependent, and we arrange this dependence to be such that, as much as possible, it fully accounts for the motion in the electronic state I in the absence of interstate coupling. Our procedure is variational in nature and, in principle, we can come as close as necessary to this ideal.

The time dependence of the coefficients $C_I(t)$ in (2.1) is therefore entirely due to interstate transitions. In our approach their time dependence is determined together with the time dependence of the nuclear wave function, $\chi_I(\mathbf{R};t)$. This is where the concept of "spawning" comes in. Spawning means adding a new basis state to the representation

$$\chi_I(\mathbf{R};t) = \sum_j d_{I,j}(t)\chi^I_j(\mathbf{R};\bar{\mathbf{R}}^I_j(t),\bar{\mathbf{P}}^I_j(t),\gamma^I_j(t),\alpha^I_j) \qquad (2.2)$$

of the nuclear wave function. We add ("spawn") another term to the sum if the effective interstate coupling requires it. In (2.2) there are again two sources of time dependence. One is the time dependence of the basis states χ^I_j. Each such state is centered about a classical trajectory (defined by its position vector, $\bar{\mathbf{R}}^I_j(t)$, momentum vector, $\bar{\mathbf{P}}^I_j(t)$, and nuclear phase $\gamma^I_j(t)$). Hence such aspects of the dynamics that are fully classical can be described by one term in the sum in (2.2). (In multidimensional problems, such as the one discussed here, each single term in the sum (2.2) is a product of one dimensional basis states, which we take to be of a Gaussian form with a time independent width, α^I_j.) The additional time dependence, as allowed for by the coefficients $d_{I,j}(t)$, has two sources. The first is the object of our interest, namely, the interstate coupling which transfers the system between different electronic states. The other and for the present, less interesting, nonclassical aspect is that even for a single electronic state there can be quantum effects in the dynamics.

In summary, before the collision, at $t \rightarrow -\infty$ one specifies the initial state. As the colliding partners approach, the only source of a time dependence is that of those nuclear basis states that were initially populated. The program monitors the effective nonadiabatic coupling, which, for the present problem, where we use a diabatic electronic basis, is given by the absolute value of the nonadiabatic coupling divided by the electronic energy gap, computed at the nuclear coordinates of the basis function representing the initial state:

$$H^{eff}_{IJ}(\mathbf{R}) = \left|\frac{\langle\phi_I(\mathbf{r}_e;\mathbf{R})|\hat{H}|\phi_J(\mathbf{r}_e;\mathbf{R})\rangle_{\mathbf{r}_e}}{E_{I,I}(\mathbf{R}) - E_{J,J}(\mathbf{R})}\right| \qquad (2.3)$$

If $H^{eff}_{IJ}(\mathbf{R})$ reaches a threshold value (preassigned and determined by numerical convergence requirements[38]) we spawn, that is, we allow a new nuclear basis state to become populated.[42] If electronic state I is populated, we spawn into state J and vice versa. In practice we even allow for "back spawning", i.e., for the back coupling from the ground to the excited state; see refs 38 and 43 for more details. Here we emphasize that the need for, and the extent of, spawning is controlled by the equations of motion (see, e.g., refs 38−40), so that the time evolution is unitary and probability is inherently conserved.

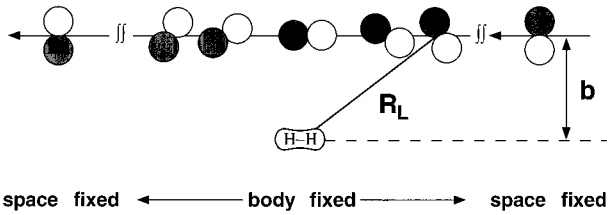

Figure 1. Schematic illustration of a collision between an atom in a ^{2}P state and a diatomic molecule at a nonzero impact parameter, b. The different orientations of the p orbital correspond to different time points during the collision. When the atom and molecule are far apart the orientation of the atomic p orbital is fixed in space. As the collision partners approach each other, a particular orientation (a p_z orbital parallel to the molecular axis) is preferred and the orbital "locks" onto the internuclear axis. As the collision partners recede from each other the orbital "unlocks" and the correlation between its orientation and the molecular axis is lost. If, as is shown here, the onset of locking and unlocking occur at a similar distance, there is a well-defined locking radius.

One could say that "spawning" is a quantum mechanical version of trajectory surface hopping,[44,45] except that the procedure is fully quantal, and the extent of bifurcation of the wave function into different electronic states is fully governed by the dynamics and is not specified by a model. It should be noted that when we spawn, we spawn into a nuclear basis state which is localized in the region of effective coupling. The spawning, as governed by the dynamics, is not instantaneous. Hence, if the system remains too long in the region of effective coupling it may be necessary to spawn more than once. It may also be necessary to back spawn into the initial electronic state. Multiple spawning will also occur if the system traverses the region of effective interstate coupling periodically, as is the case for our problem, particularly so with respect to the quenching process.[37,38] The back and multiple spawning in the case of quenching for $Na^* + H_2$ leads to random walk-like changes in the population on the ground electronic state.

3. Orbital Following and Nonadiabatic Transitions

The concept of orbital following has been amply discussed in the literature for atom−atom collisions.[12,13,46−52] Our discussion centers on the atom−molecule case, with special emphasis on the relationship to concepts of adiabaticity and nonadiabatic transitions. In Figure 1, we present a caricature of the basic phenomenon for an atom in a ^{2}P state colliding with a diatomic molecule. The p orbital of the atom may be randomly oriented with respect to the molecular axis at the start of the collision. As the atom and molecule approach, one particular orientation of the p orbital may be preferred—in the case of $Na^* + H_2$, it is the one where the p orbital is parallel to the molecular axis. If this preference is sufficiently strong, it may happen that the p orbital "locks" on the preferred orientation at some atom−molecule distance and maintains this locked position during the collision. As the atom and molecule separate, the correlation between the orientation of the p orbital and that of the molecular axis will be lost. If this occurs at the same, or a similar, atom−molecule distance as the onset of locking, we may define a "locking radius". We will refer to this limiting case as perfect

locking. In the opposite limit, the p orbital orientation is fixed in space and independent of the molecular axis throughout the entire collision.

It is apparent that in the case of perfect locking, the molecular frame provides the natural representation for the dynamics during the collision, while in the opposite limit it is the lab frame that is most appropriate. This is because the definition of the relevant electronic states depends on the choice of frame. For example, if we choose the lab frame, the state $Na(3p_Z)-H_2$ corresponds to a space-fixed p orbital throughout the collision. On the other hand, in the molecular frame the state $Na(3p_z)-H_2$ corresponds to a p orbital which has a predefined (we take it as parallel in the coordinate system used below) orientation relative to the H_2 molecular axis. We have used capital and lower-case subscripts to denote the lab and molecular frames, respectively, and will continue to do so throughout. (As discussed in detail in section 4. A, our choice of the body frame coordinate system is such that the *z* axis coincides with the H−H molecular axis and the Na−H_2 system lies in the *x*−*z* plane.) An important point is that *neither* of these frames is necessarily coincident with an adiabatic description of the electronic states. Instead, they are both diabatic representations and, in the absence of electronic transitions, neither exactly describes the situation where the electron instantaneously adjusts to the energetically preferred orientation.

The lab frame is most natural for large impact parameters, where the atom and molecule interact only weakly and the p orbital is hardly perturbed. Thus, when there is no orbital following, the amplitudes of the electronic states are constant in the lab frame. On the other hand, if there is perfect locking for all atom−molecule distances, the amplitudes of the electronic states are constant in the molecular frame. One should not overlook the fact that there are both kinetic and potential energy interstate couplings in the molecular frame, the former being essentially kinematic and arising from the time-dependence of the R matrix given below. The space-fixed frame may also have kinetic energy interstate couplings, but these are expected to be rather small since the p orbitals are independent of atom−molecule orientation.

In the realistic case, electronic transitions will occur at some point in either frame. Before the collision, when the atom and molecule are far apart, the orbital is space-fixed and thus in the molecular frame the electronic state amplitudes must change to reflect any rotation of the molecule. On the other hand, the orbital must reorient during the locking time and thus there will be electronic transitions during this time in the lab frame. Note that in the atom−atom case one expects the orbital to lock onto the atom−atom relative coordinate, *R*, whereas here, and by analogy to the stereodynamics of oriented molecules, we expect that at lower impact parameters the orbital will lock onto the axis, *r*, of the diatomic molecule. This is also in accord with the potential seen by the p_z orbital, cf. the right panel of Figure 2. These considerations represent added complications relative to orbital locking as discussed for atom−atom collisions.[52,53]

4. Orbitals and Potentials in the Na* + H_2 System

The chemical physics of the Na* + H_2 collision is most easily described in the body fixed system of coordinates where electronic states can be classified by symmetry.[22,25,26,54] Two technical aspects that need discussion are the transformation of the p atomic orbitals from the space-fixed to the body-fixed system of coordinates and the use of these orbitals to specify an approximate analytical form for the potential energy.

A. Potential Energy Surfaces. There are four low-lying electronic states of Na + H_2—the ground state with the valence electron of Na in a 3s orbital and the three states arising from placing the valence electron in a 3p orbital. In this paper, we are not concerned with the Na(3s) + H_2 state, which is involved in quenching of the electronically excited state. Nevertheless, we point out that the computations do include this state and permit discussion of both quenching (Na(p) → Na(*s*) transitions) and orbital following ($Na(p_i) \rightarrow Na(p_j)$ transitions). Our potential is derived from considerations of angular overlap[55] and parametrized with reference to earlier *ab initio* calculations.[22−25] In particular, we invoke the approximation that the strength of bonding and antibonding interactions is in first order proportional to the square of the overlap between any two orbitals. In the following brief discussion, we limit consideration to the three valence electrons of Na + H_2 and we do not discuss the Na(3s) + H_2 state, which, however, is retained in the computation—including its coupling to the $Na(3p_z)$ + H_2 and $Na(3p_x)$ + H_2 states. The explicit form of the potential surfaces and their couplings, including the detailed numerical parameters used, have been presented previously.[38] Representing H_2 with two molecular orbitals, σ and σ^*, it is seen that any overlap of a Na(3p) orbital with the fully occupied σ orbital will lead to antibonding, i.e., Pauli repulsion. On the other hand, overlap with the σ^* orbital allows for delocalization of the Na electron and a concomitant lowering of its kinetic energy. At this point we specify the coordinate system for further discussion as one in the molecular frame, where *r*, *R*, and γ denote the H−H distance, Na−H_2 (center of mass) distance, and the angle γ between *r* and *R*. The *z* axis is chosen parallel to the H−H molecular axis and the Na−H_2 molecule lies in the *x*−*z* plane. With these definitions, the p_y orbital always has zero overlap with both of the H_2 molecular orbitals. On the other hand, the p_x and p_z orbitals will be repulsive or attractive in varying degrees according to the angle γ. In C_{2v} symmetry, the p_x state is repulsive and the p_z state has a shallow well. In $C_{\infty v}$ symmetry, the p_z orbital overlaps with both of the H_2 MO's, while the p_x orbital is orthogonal to both. One therefore expects stronger Pauli repulsion in the p_z state. This implies that the energetic ordering of the p_z and p_x states is reversed as γ is varied from 0 ($C_{\infty v}$) to $\pi/2$ (C_{2v}) to π ($C_{\infty v}$). Because these states have the same symmetry labels in C_s, they may exhibit an avoided crossing. In contrast, the p_y orbital has a different symmetry label in all three possible groups, i.e., for all γ. Hence, it is rigorously uncoupled from the p_x and p_z states. All of these qualitative considerations are borne out by detailed *ab initio* computations.[22−25]

In Figure 2, we show the potential energy surfaces for the p_x and p_z states in the molecular frame diabatic representation described above. The H−H distance is fixed to its equilibrium value, and the seam along which the two states are degenerate is indicated with a thick line. The potential energy surfaces are qualitatively different for approach along $C_{\infty v}$ and C_{2v} symmetry. In particular, the lower energy p_z state favors a perpendicular arrangement (C_{2v}), while the p_x state favors a parallel arrangement ($C_{\infty v}$). These differences are a determining factor in the stereochemistry of orbital following. Notice in particular the well in the p_z state—it is the attractive branch of this well which provides the impetus for orbital following. Picturesquely, the Na atom is captured in this well and perfect orbital locking would imply that it was fixed at the bottom of the well for the duration of the collision.

Unfortunately, there is little quantitative information about the interstate coupling. Hence, we have simply used a functional form which is consistent with the symmetry-imposed requirement that the coupling is continuous and vanishes in the C_{2v} and $C_{\infty v}$ nuclear configurations and at large Na−H_2

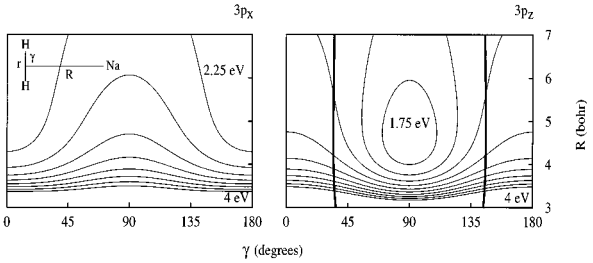

Figure 2. Molecular frame diabatic potential energy surfaces for the $3p_x$ (left panel) and $3p_z$ (right panel) states as a function of the bending angle, γ, and the Na−H_2 distance, R (in bohr). (See inset in left panel.) In both panels the H−H distance is fixed to its equilibrium value and energy is measured (in eV) from the ground state, i.e., a Na (3s) atom and H_2 at r_{eq}, far apart and at rest. The contours are equally spaced (0.25 eV apart) and the lowest and highest values are indicated in each panel. The thick line in the right panel indicates the seam along which the two surfaces are degenerate. At both C_{2v} and $C_{\infty v}$ symmetries the two surfaces are qualitatively different and in particular whereas the $3p_z$ surface has a well in C_{2v} symmetry, the $3p_x$ surface is repulsive at this configuration and favors the $C_{\infty v}$ arrangement. Perfect locking occurs when the electron stays in a $3p_z$ state. Failure to track the rotation of the H_2 axis is a nonadiabatic transition to the $3p_x$ state. Therefore, the qualitative differences between the surfaces shown, and the long seam along R, are incisive in the stereodynamics of orbital following.

and H−H separations:

$$V_{p_x-p_z}(r, R, \gamma) = \lambda \sin(2\gamma) \exp(-\alpha_r r) \exp(-\alpha_R R) \qquad (4.1)$$

The parameters for the potential energy surfaces and couplings used have been given previously,[38] and here we just quote those parameters used for the coupling between the p_x and p_z states, eq 4.1, (in atomic units, $\lambda = 0.12$, $\alpha_r = 0.5$, $\alpha_R = 0.25$). As we shall discuss, these parameters allow the electrons to lag behind the nuclear motion, thereby leading to a rather long onset of orbital locking. (See Figures 4−6.) Note that, by symmetry, the Na($3p_y$)−H_2 state is rigorously uncoupled for all nuclear configurations. This is of course only true in the molecular frame, and in general all three states are coupled in the lab frame.

B. Lab and Molecular Frames. The actual computations are done in the space-fixed frame rather than the molecule-fixed frame which we have used to describe the potential energy surfaces. Furthermore, we use a Cartesian coordinate system with no reduction in dimensionality. In contrast to most quantal treatments of molecular dynamics, the three redundant degrees of freedom corresponding to center-of-mass motion are not removed. From the point of view of computational effort, this is therefore a nine-dimensional calculation. We feel that the increase in dimensionality is a minor price to pay in view of the resulting simplicity and generality in the equations of motion—a conclusion which was agreed upon long ago in classical molecular dynamics.[56] It is the use of classical mechanics as a guiding force in basis set selection, avoiding the exponential scaling behavior of many quantal dynamics methods,[57] that makes this choice practical in our method.

The molecular frame can constantly tumble in the space fixed frame. There will therefore be a rotation matrix R,[58] describing the orientation of the Na*−H_2 exciplex in space, which will transform between the two bases, of the three p orbitals

$$\begin{pmatrix} 3p_X \\ 3p_Y \\ 3p_Z \end{pmatrix}_{\text{Lab}} = R \begin{pmatrix} 3p_x \\ 3p_y \\ 3p_z \end{pmatrix}_{\text{Body}},$$

$$R = \begin{pmatrix} \cos\phi\cos\theta & -\sin\phi & \cos\phi\sin\theta \\ \sin\phi\cos\theta & \cos\phi & \sin\phi\sin\theta \\ -\sin\theta & 0 & \cos\theta \end{pmatrix} \qquad (4.2)$$

The elements of the matrix R can be determined, whenever needed, because in the actual computation the atoms are specified by their position in the lab system (which determines the polar, θ, and azimuthal, ϕ, angles in eq 4.2).

5. Results

Our computations have been designed to model the experimental scenario where Na atoms are excited by light which is linearly polarized along a fixed axis in the lab frame at the wavelength of the Na D line (∼2.1 eV). (Note that we ignore the hyperfine structure of the Na atom, m_F, which broadens the distribution of initial states.) These excited Na atoms then impinge on a gas of H_2 molecules, and we monitor both the electronic quenching and the orbital reorientation occurring during the collision. The simulations begin with Na* and H_2 outside of the interaction region (separated by ≈30 bohr), H_2 randomly oriented, and 0.039 eV of relative kinetic energy. A single trajectory (nuclear basis function) is used to model the initial conditions—hence, the initial state is nonstationary and corresponds to a coherent vibrational state and pendular rotational state[59] of H_2 and a translational wavepacket for the excited Na atom.

The nonstationary nature of the underlying basis is required in order to maintain the classical underpinning of the method discussed above and is entirely appropriate when considering ultrafast excitation, for example, pump−probe spectroscopy.[60−62] However, we are also interested in the historically more common experiments which do not use ultrashort laser pulses, and in such cases the initial state is generally a stationary one. In order to mimic these cases, one should in principle decompose the initial state into a sum over nonstationary states and either begin the simulations with more than one nuclear basis function populated or coherently sum the time-evolved wave functions (weighted by the appropriate amplitudes) for these nonstationary states. When one is interested in expectation values of observables, we have found that it is often sufficient to replace the final coherent sum of wave functions with an incoherent sum. Any expectation value is then a weighted average of expectation values for each of the time-evolved nonstationary initial states. This is not the same as the usual classical averaging procedure, because each of the nonstationary initial states is propagated quantum mechanically, retaining full account of quantal interference with the basis functions it spawns. Instead, it represents a partial classical averaging which retains the short-time quantal interference which is absolutely necessary to describe nonadiabatic events (coherences between trajectories and the trajectories they spawn), while coarse-graining over the longer-time coherences between trajectories which represent varying initial conditions. A distinct advantage of this procedure, as compared to one where an initial stationary state is represented directly by a set of initial nonstationary states (all initially populated), is that one has direct access to a classical-like picture of the dynamics, which is, however, modified by quantal considerations. This greatly aids in our understanding of the results.

In the following analysis of the results, expectation values obtained from the evolution of a single nonstationary initial state are referred to as originating from "single runs", in contrast to those incoherently averaged expectation values which correspond to a stationary initial state. The stationary initial states modeled correspond to H_2 (v=0, j=0) and H_2 (v=0, j=3). The latter is appropriate for considering experiments at elevated temperatures of 700 K.

The expectation value of interest with regard to orbital following is the projection angle that the Na p orbital makes

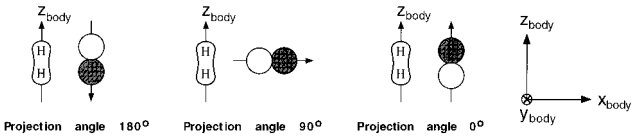

Figure 3. Projection angle of the Na p orbital on the H_2 molecular axis. The z (body frame) axis coincides with the H-H molecular axis and the Na$-H_2$ system lies in the $x-z$ plane. Perfect locking occurs when the angle is either zero or π, but as discussed in the text the range of physically distinguishable angles extends only from zero to $\pi/2$.

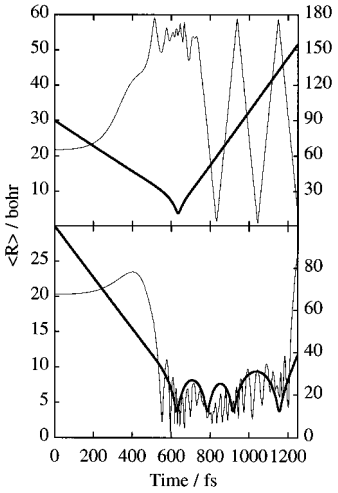

Figure 4. Expectation values of the Na$-H_2$ distance (thick line and left axis) and of the bending angle, γ (thin line and right axis), as a function of time in femtoseconds at two impact parameters: 4 bohr (upper panel) and 2 bohr (lower panel). In both panels the H_2 molecule is initially in a coherent vibrational state and a pendular rotational state (drawn from a $v = 0, j = 0$ distribution), and the relative kinetic energy in the collision is set to 0.039 eV. The zero of time is defined arbitrarily for the reactants separated by ≈30 bohr. At low−moderate values of the initial impact parameter ($b < 8$ bohr) this is typically what we see for these initial collision parameters: at early times the projection angle is nearly constant because the H_2 molecule is initially rotationless, whereas due to collision-induced rotational excitation it may vary periodically after the collision, as is most evident in the upper panel. Locking is indicated by an oscillatory motion about an angle of zero or π (see Figure 3). As discussed in the text, the locking is not perfect. At lower impact parameters a long-lived collision complex is sometimes formed (lower panel), in which case the locking lasts for a longer time, extending over a few H_2 rotational periods.

with the H_2 molecular axis. In the absence of electronic transitions in the manifold of p states, this would be the same as the projection angle of the H_2 molecular axis on the lab frame. Thus for initially rotationless H_2, it would be constant until the Na* and H_2 entered the interaction region. On the other hand, after the collision is over, it will be changing to reflect the collision-induced rotational excitation of H_2. In Figure 3, we show a caricature which clarifies this projection angle. In particular, note that it varies from 0 to π (where the two extremes correspond to perfect locking, compare to Figure 1), but the range of physically distinguishable angles only extends from 0 to $\pi/2$. That is to say, the phase of an aligned p orbital is arbitrary, and we have incorporated this symmetry correctly in the averaged results presented below.

Figure 4 presents the results of single runs which demonstrate the orbital locking for two impact parameters (or equivalently, two values of the total angular momentum of Na*$-H_2$), $b = 4$ bohr (upper panel) and $b = 2$ bohr (lower panel). These are representative of many such single runs (averaged results corresponding to an initial stationary state are presented later). The expectation values of the projection angle and the Na*$-H_2$ distance are shown as a function of time. In this and other plots of single runs, the results are typical and not strongly dependent on initial conditions.

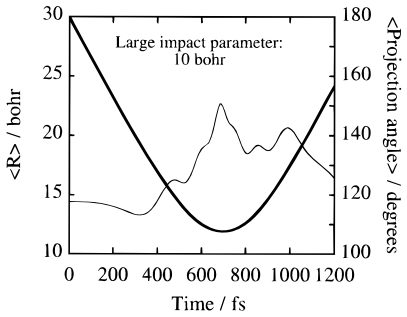

Figure 5. Same as Figure 4 but at a large impact parameter of 10 bohr where in a typical run (such as the one shown here) locking is much less pronounced (when compared to single runs at low−moderate impact parameters; see Figure 4). At large impact parameters the Na p orbital interacts only weakly with the molecule (compare the distance of closest approach shown here to that shown in figure 4) and therefore we do not expect to see a strong propensity for alignment.

Because the H_2 molecule is initially rotationless, the projection angle in both cases is nearly constant during the Na$-H_2$ approach. On the other hand, it varies periodically as the Na* and H_2 recede from each other. This is a consequence of the collision-induced rotational excitation of the H_2 molecule and is seen most clearly in the upper panel. (Note that although the projection angle changes periodically, when the molecule is rotationally excited, its range of variation is in general not from 0 to π because the molecular axis and the orbital axis need not necessarily be in the same plane, and furthermore, more than one basis function may contribute to the expectation value that we show.) Perfect locking would be indicated by a projection angle of either 0 or π during the collision. There are two deviations from this idealized picture. The projection angle never reaches 0 or π and it oscillates rather than remaining fixed during the collision. These deviations arise because the electronic motion corresponding to orbital reorientation is not perfectly adiabatic. The majority of the nuclear population undergoes the electronic transitions necessary for orbital following, but some portion proceeds diabatically. In effect, there is some probability for the orbital to "slip" out of the grasp of the H_2 molecular axis. The expectation value of the projection angle that we show contains contributions from both the diabatic and adiabatic populations, and the small amount which proceeds diabatically prevents it from reaching 0 or π. The oscillations come about from two sources. That portion of the nuclear population which is proceeding diabatically, i.e., in a space-fixed frame, will give rise to an oscillating contribution to the projection angle, reflecting the nascent rotation of the H_2 molecule. Furthermore, even that portion of the population which proceeds adiabatically contributes an oscillatory signal because there is some kinetic energy in the bending motion of the Na*$-H_2$ complex. The collision shown in the lower panel leads to a long-lived complex, and we see this very often for lower impact parameters. However, one should recall that there is simultaneously electronic quenching (to the Na(3s) + H_2 state) which we are not discussing. Hence, the population of any long-lived complex is decaying by nonadiabatic transitions to the ground state. From these two panels, one can estimate the locking radius between 10 and 15 bohr.

A single run which is typical of larger impact parameters (10 bohr in this example) is shown in Figure 5. There is an attempt at locking—the peak near $t = 700$ fs. However, the projection angle only reaches 150° indicating that the electronic nonadiabatic transitions are far from perfect and much of the

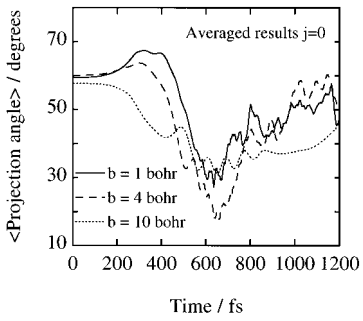

Figure 6. Expectation value of the projection angle as a function of time (in femtoseconds) for H_2 that is initially at $v = 0$, $j = 0$ and at three impact parameters: 1 bohr (full line), 4 bohr (dashed line), and 10 bohr (dotted line). At each impact parameter the results are averaged over 40 runs, and the relative kinetic energy is as in Figures 4 and 5. Even for the averaged results, locking is easily discerned at not too large values ($b < 8$ bohr) of the initial impact parameter, and it is most pronounced at an impact parameter of 4 bohr. At large impact parameters (10 bohr, dotted line) the motion is more adiabatic (because the velocity along the approach coordinate is lower since the relative kinetic energy is the same and the centrifugal barrier increases), yet the Na p orbital interacts only weakly with the molecule (because of the repulsive centrifugal term that prevents the atom from closely approaching the molecule; see Figure 5), and therefore the lab frame coordinate system becomes more natural for describing such collisions.

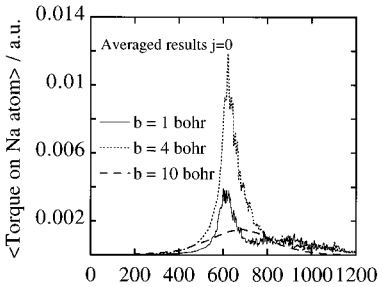

Figure 7. Expectation value of the torque on the Na* atom about the center of mass of the H_2 molecule for three impact parameters averaged to correspond to H_2 initially in a $v = 0$, $j = 0$ stationary state. Compare with Figure 6 and note that the efficiency of locking is correlated with large values of this torque.

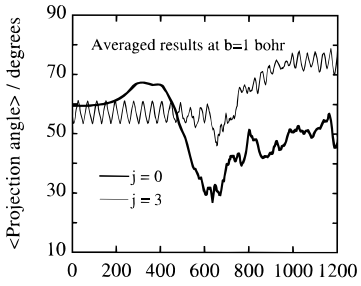

Figure 8. Same as Figure 6 but for a single value of the initial impact parameter, 1 bohr, and for H_2 that is initially at $v = 0$, $j = 0$ (thick line) and $v = 0$, $j = 3$ (thin line). As in Figure 6, the results are averaged over 40 runs (for each initial state). Although there is still some tendency to lock at $j = 3$ it is much less pronounced than at $j = 0$ and the motion is basically nonadiabatic: the electronic motion fails to track the nuclear rotational motion. The oscillatory motion before the attempt to lock (at $j = 3$) should average to zero for a stationary initial state. Its amplitude, $\pm 5°$, serves as a measure for our statistical uncertainty.

wavepacket proceeds in a space-fixed manner, i.e., diabatically. At such large impact parameters, the atom and molecule interact only weakly, because of the repulsive centrifugal term that prevents the Na atom from closely approaching the H_2 molecule. Therefore, we expect locking to be inefficient. That there is any locking at all is a reflection of the fact that the attractive basin of the p_z excited state extends out to rather large distances (see the second contour in Figure 2 drawn at a value of 2 eV, which is below the asymptotic value of the Na D line, ~2.1 eV).

After examination of the behavior of individual runs, it is natural to inquire about the behavior for a stationary initial state. One of course expects a "washing out" of the finer structure seen in the single runs, and this is observed. In Figure 6, we show the expectation value of the projection angle for an incoherent average of 40 single runs for various impact parameters with the initial conditions for the nonstationary initial basis functions chosen from a distribution corresponding to Na* + H_2 (v=0, j=0). The locking is most nearly perfect for b = 4 bohr and it is less efficient (although not absent) at 10 bohr for the reasons discussed in the previous paragraph. On the basis of Figures 4−6 we can conclude that the lab frame coordinate system is most natural at impact parameters >15 bohr where the system does not enter the locking regime and the Na* p orbital is not significantly perturbed by the molecule.

It is interesting that locking is more efficient at intermediate impact parameters. The physical reason for this is that the impact parameter, b, determines the rate of rotation of the vector **R** connecting the Na atom to the center of mass of the H_2 molecule. In the absence of forces, **R** rotates at the angular speed of[63] $\psi = bv/\mathbf{R}^2$, which is faster than the rotation of H_2, except at very low impact parameters. (To see this compare $\psi = L/\mu\mathbf{R}^2$ to j/I where I is the moment of inertia, L is the angular momentum along the atom−molecule approach coordinate, and j is the angular momentum of H_2. Heavier diatomics, for which I is far larger, will rotate even more slowly than H_2. It is therefore the rotation of **R** that determines the change of the angle γ with time. The torque on the orbital is determined by the variation of the potential with γ, cf. Figure 2, and hence locking is favored at such impact parameters that are not too small, yet not so large that they exclude the system from the range in **R** where the potential is appreciable (four to six atomic units). This argument can be expressed in terms of the torque exerted on the Na* atom (about the center of mass of the H_2 molecule) during the collision, which provides an indicator of the force directing the Na−H_2 complex into C_{2v} symmetry. Because this is the geometry which is preferred for orbital locking, the magnitude of this torque specifies the degree of locking. The torque arises from a competition between two factors—the b-dependent length of the lever arm (Na−H_2 distance) and the force exerted on the Na* atom. In maximizing the magnitude of the torque, the first factor favors large impact parameters, while the second favors small impact parameters. Thus, maximal torque is achieved for intermediate impact parameters. These arguments are confirmed by Figure 7, where the instantaneous expectation value of the torque is shown for the same three values of the impact parameter used in Figure 6. Note that the ordering of impact parameters by the magnitude of the torque is indeed the same as the ordering by locking efficiency from Figure 6.

Figure 8 compares the average projection angle for stationary initial states corresponding to $v = 0$, $j = 0$ and $v = 0$, $j = 3$ at an impact parameter of 1 bohr. Initial rotational excitation of the H_2 molecule makes it harder for the orbital to lock on the molecular axis. This would be entirely expected if the locking motion were that of a classical quadrupole, but we remind the reader that orbital locking is an electronic motion. Hence, what we are seeing here is the failure of the electronic motion to track the nuclear motion on a time scale of 100 fs (rotational period of H_2 in $j = 3$). This is rather long on the electronic

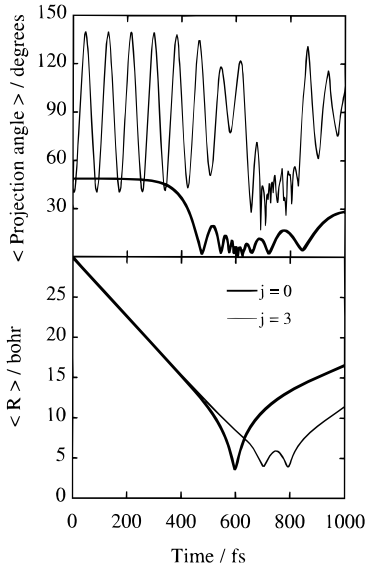

Figure 9. Comparison between single (different) runs at an impact parameter of 1 bohr and for pendular states of H_2 drawn from $j = 0$ (thick line) and $j = 3$ (thin line) distributions. In both runs the H_2 molecule is initially in a coherent vibrational state drawn from a $v = 0$ distribution. Upper panel, expectation value of the projection angle; lower panel, expectation value of the Na−H_2 distance vs time in femtoseconds. As is evident from the upper panel, it takes the p orbital about 200 fs to reorient and align along the molecular axis. This rotation time is slower than the H_2 ($j = 3$) rotational period (∼100 fs) and hence the failure to lock when the H_2 is initially rotationally excited.

time scale, and thus the nonadiabaticity is slightly unexpected. Even so, one can discern some propensity for locking when $j = 3$. The oscillations which are present before and after the apparent attempt at locking (between 600 and 800 fs) are the signature of the H_2 rotation. Because the initial angle γ is chosen randomly, these oscillations, which are pronounced in single runs (see, e.g., the upper panel of Figure 4) should average to zero amplitude before the collision when the H_2 molecule is in a stationary rotational state. Hence, the amplitude of these oscillations provides a measure of our statistical uncertainty, which appears to be about ± 5°.

In order to investigate further the failure of locking when H_2 is initially rotationally excited, we compare the projection angle for two single runs in the upper panel of Figure 9. The thick and thin lines describe a pendular state of H_2 drawn from the $j = 0$ and $j = 3$ distributions, respectively. In the lower panel, we show the expectation value of the Na−H_2 distance so that the reader can see when the collision is occurring. As in the averaged results presented in Figure 6, the impact parameter is chosen to be 1 bohr. Looking at the variation of the projection angle for $j = 0$, we see that it begins to lock around $t = 300$ fs and the locking is essentially complete by $t = 500$ fs. The "locking time" can thus be estimated as 200 fs, which is longer than the rotational period of H_2 for $j = 3$ (100 fs). The reader can verify that this estimate of the locking time is consistent with the data in Figures 4 and 5. The averaged results presented in Figure 6 lead to a slightly longer estimate, but this is because there is a distribution of collision times which makes it more difficult to estimate a meaningful locking time. In any case, one can see from the upper panel of Figure 9 that the locking takes longer than the rotational period of H_2 ($j = 3$). This is the source of the decreased locking efficiency for H_2 which is initially rotationally excited—the rotation of the electronic p orbital is not instantaneous but takes nearly 200 fs, and when H_2 is rotating faster than this, the p orbital cannot lock. The reason there is any locking at all is certainly because the rotation of H_2 is hindered during the collision (because the Na* atom is in its way, and furthermore in this specific example a short lived Na*−H_2 complex was formed).

6. Concluding Remarks

Orbital following in the collision of a Na (3p) atom and an H_2 molecule was discussed with special emphasis on electronically nonadiabatic transitions. We find that the picture of orbital reorientation which has been advanced by Hertel et al. is valid, with some modifications. First, it must be recognized that the quantum mechanical nature of nonadiabatic transitions will lead to a "smearing" of the classical picture. For example, there is no single well-defined "locking radius" or "locking time". However, these concepts are still approximately valid, e.g., the locking typically occurs in a range of Na−H_2 distances between 10 and 15 bohr. Unlike the electronic quenching in this same molecule, which proceeds in many small yet distinct bursts, the reorientation of the p orbital is much more nearly continuous. In large part, this is because the near degeneracy of the p_x and p_z states is dependent only on the bending angle and Na−H_2 distance in the Na*−H_2 complex, while the intersection of the ground and p_z states (through which the quenching occurs) depends also on the H−H bond being extended. Therefore, there are only two "clocks" governing the frequency of nonadiabatic transitions corresponding to orbital reorientation, while there are three in the case of quenching.[37,38]

The second refinement of the classical picture recognizes that the locking is not perfect. We see quite clearly that the orbital oscillates about the locked orientation (because there is some kinetic energy in the bending motion of the Na*−H_2 complex) and the expectation value of the projection angle does not usually reach the values of 0 or π that are expected in the ideal case. This is again due to the nonclassical nature of the realistic picture, where there is rarely complete population transfer between electronic states corresponding to orbital reorientation. Instead, some pieces of the wavepacket align and others proceed on the same electronic state.

A third point is the role of the torque on the Na* atom as an important variable which governs the locking. This torque gives a measure of the tendency of the complex to adopt the C_{2v} symmetry, which most favors orbital locking. Because the magnitude of this torque arises from two competing factors (the Na−H_2 distance that favors large impact parameters and the force exerted on the Na* atom that favors small impact parameters), the locking is most efficient at intermediate impact parameters.

Finally, we note that the electronic reorientation takes a remarkably long time—often over 100 fs, e.g., Figures 4−6. Because of this, locking becomes less efficient when the H_2 molecule is rotationally excited, Figure 8. Given the Born−Oppenheimer assumption that electrons move much faster than nuclei, this might seem surprising, except of course that the nonadiabatic transition occurs between two excited states which are nearly degenerate over a wide range in R, Figure 2. The locking time would decrease significantly if the interstate coupling were stronger so that the adiabatic states were further apart. Since there is no ready source of information regarding these couplings, we cannot predict whether this "slow electronic motion" is in fact the case in Na* + H_2. It will be interesting to see whether this conclusion remains using *ab initio* nonadiabatic molecular dynamics, where the couplings and potential energy surfaces are generated from first principles.[64] Returning to our opening question, a nonadiabatic orbital reorientation is expected to be a general phenomenon when the coupling among excited p states is not strong.

Acknowledgment. We thank E. E. B. Campbell, I. V. Hertel, K. L. Kompa, and M. Motzkus for discussions and H.-J. Loesch and J. Hinze for the invitation to present our work. M.B.N. is grateful to the US−Israel Binational Foundation for a Fulbright fellowship and to the Rothschild Foundation for a Postdoctoral Fellowship. T.J.M. thanks the University of Illinois Department of Chemistry for initial funding. This work was supported in part by an Air Force Office of Scientific Research grant to R.D.L.

References and Notes

(1) Teller, E. *J. Phys. Chem.* **1937**, *41*, 109.
(2) Teller, E. *Isr. J. Chem.* **1969**, *7*, 227.
(3) Baer, M. *J. Phys. Chem.*, this issue.
(4) Schnieder, L.; Seekamp-Rahn, K.; Borkowski, J.; Wrede, E.; Welge, K. H.; Aoiz, F. J.; Banares, L.; D'Mello, M. J.; Herrero, V. J.; Saez-Rabanos, V.; Wyatt, R. E. *Science* **1995**, *269*, 207.
(5) Neuhauser, D.; Judson, R. S.; Kouri, D. J.; Adelman, D. E.; Shafer, N. E.; Kliner, D. A.; Zare, R. N. *Science* **1992**, *257*, 519.
(6) Wu, Y. S.; Kuppermann, A. *Chem. Phys. Lett.* **1995**, *235*, 105.
(7) D'Mello, M. J.; Manolopoulos, D. E.; Wyatt, R. E. *Science* **1994**, *263*, 102.
(8) Wu, Y. S.; Kuppermann, A. *Chem. Phys. Lett.* **1993**, *205*, 105.
(9) Wu, Y. S.; Kuppermann, A. *Chem. Phys. Lett.* **1993**, *213*, 636.
(10) Woodward, R. B.; Hoffman, R. *The Conservation of Orbital Symmetry*; Verlag Chemie: Weinheim/Deerfield Beach, 1970.
(11) Hertel, I. V. *Adv. Chem. Phys.* **1981**, *45*, 341.
(12) Hertel, I. V.; Schmidt, H.; Bahring, A.; Meyer, E. *Rep. Prog. Phys.* **1985**, *48*, 375.
(13) Rettner, C. T.; Zare, R. N. *J. Chem. Phys.* **1981**, *75*, 3636.
(14) Loesch, H. J. *J. Chem. Phys.* **1986**, *104*, 213.
(15) Loesch, H. J. *J. Chem. Phys.* **1987**, *112*, 85.
(16) Bernstein, R. B.; Levine, R. D. *J. Phys. Chem.* **1989**, *93*, 1687.
(17) Levine, R. D. *J. Phys. Chem.* **1990**, *94*, 8872.
(18) Campbell, E. E. B.; Schmidt, H.; Hertel, I. V. *Adv. Chem. Phys.* **1988**, *72*, 37.
(19) Reiland, W.; Tittes, U.; Hertel, I. V. *Phys. Rev. Lett.* **1982**, *48*, 389.
(20) Reiland, W.; Jamieson, G.; Tittes, U.; Hertel, I. V. *Z. Phys. A* **1982**, *307*, 51.
(21) Poppe, D. *Z. Phys. D* **1986**, *1*, 207.
(22) Botschwina, P.; Meyer, W.; Hertel, I. V.; Reiland, W. *J. Chem. Phys.* **1981**, *75*, 5438.
(23) Nielsen, S. E.; Dahler, J. S. *J. Phys. B* **1976**, *9*, 1383.
(24) Nielsen, S. E.; Dahler, J. S. *J. Phys. B* **1980**, *13*, 2435.
(25) Vivie-Riedle, R. d.; Hering, P.; Kompa, K. L. *Z. Phys. D.* **1990**, *17*, 299.
(26) Halvick, P.; Truhlar, D. G. *J. Chem. Phys.* **1992**, *96*, 2895.
(27) Motzkus, M.; Pedersen, S.; Zewail, A. H. *J. Phys. Chem.* **1996**, *100*, 5620.
(28) Blais, N. C.; Truhlar, D. G. *J. Chem. Phys.* **1983**, *79*, 1334.
(29) Truhlar, D. G.; Duff, J. W.; Blais, N. C.; Tully, J. C.; Garrett, B. C. *J. Chem. Phys.* **1982**, *77*, 764.
(30) Tawa, G. T.; Mielke, S. L.; Truhlar, D. G. *J. Chem. Phys.* **1994**, *100*, 5751.
(31) Clary, D. *Mol. Phys.* **1984**, *53*, 1.
(32) Su, T.; Bowers, M. T. *Int. J. Mass. Spectrom. Ion Phys.* **1975**, *17*, 309.
(33) Su, T.; Bowers, M. T. In *Gas Phase Ion Chemistry;* Bowers, M. T., Ed.; Academic Press: New York, 1979.
(34) Kern, K.; Schlier, C. *Z. Phys. D* **1986**, *1*, 391.
(35) Dashevskaya, E. I.; Nikitin, E. E.; Troe, J. *J. Chem. Phys.* **1990**, *93*, 7803.
(36) Dashevskaya, E. I.; Nikitin, E. E.; Troe, J. *J. Chem. Phys.* **1992**, *97*, 3318.
(37) Ben-Nun, M.; Martínez, T. J.; Levine, R. D. *Chem. Phys. Lett.* **1997**, *270*, 319.
(38) Martínez, T. J.; Ben-Nun, M.; Levine, R. D. *J. Phys. Chem. A* **1997**, *101*, 6389.
(39) Martínez, T. J.; Ben-Nun, M.; Levine, R. D. *J. Phys. Chem.* **1996**, *100*, 7884.
(40) Martínez, T. J.; Ben-Nun, M.; Ashkenazi, G. *J. Chem. Phys.* **1996**, *104*, 2847.
(41) Martínez, T. J.; Levine, R. D. *J. Chem. Soc. Faraday Trans.* **1997**, *93*, 941.
(42) For the particular problem presented in this paper, our numerical tests have indicated that a threshold of 0.3 is sufficient to achieve convergence.
(43) Martínez, T. J.; Ben-Nun, M. *J. Chem. Phys.*, submitted.
(44) Tully, J. C. In *Dynamics of Molecular Collisions Part B;* Miller, W. H., Ed.; Plenum Press: New York, 1976.
(45) Tully, J. C. *J. Chem. Phys.* **1990**, *93*, 1061.
(46) Rettner, C. T.; Zare, R. N. *J. Chem. Phys.* **1982**, *77*, 2416.
(47) Smith, C. J.; Driessen, J. P. J.; Eno, L.; Leone, S. R. *J. Chem. Phys.* **1992**, *96*, 8212.
(48) Smith, C. J.; Spain, E. M.; Dalberth, M. J.; Leone, S. R.; Driessen, J. P. J. *J. Chem. Soc. Faraday Trans.* **1993**, *89*, 1401.
(49) Pouilly, B.; Alexander, M. H. *J. Chem. Phys.* **1987**, *86*, 5373.
(50) Pouilly, B.; Robbe, J. M.; Alexander, M. H. *J. Chem. Phys.* **1989**, *91*, 1658.
(51) Vivie-Riedle, R.; Driessen, J. P. J.; Leone, S. R. *J. Chem. Phys.* **1993**, *98*, 2038.
(52) Alexander, M. H.; Pouilly, B. *J. Chem. Phys.* **1989**, *90*, 5373.
(53) Kovalenko, L. J.; Leone, S. R.; Delos, J. B. *J. Chem. Phys.* **1989**, *91*, 6948.
(54) Yarkony, D. R. *J. Chem. Phys.* **1986**, *84*, 3206.
(55) Burdett, J. K. *Molecular Shapes: Theoretical Models of Inorganic Stereochemistry*; Wiley: New York, 1980.
(56) Allen, M. P.; Tildesley, D. J. *Computer Simulations of Liquids*; Clarendon Press: Oxford, 1992.
(57) Kosloff, R. *Annu. Rev. Phys. Chem.* **1994**, *45*, 145.
(58) Zare, R. N. *Angular Momentum*; Wiley-Interscience: New York, 1988.
(59) Rost, J. M.; Griffin, J. C.; Friedrich, B.; Herschbach, D. R. *Phys. Rev. Lett.* **1992**, *68*, 1299.
(60) Zewail, A. H. *J. Phys. Chem.* **1996**, *100*, 12701.
(61) Fleming, G. R. *Chemical Applications of Ultrafast Spectroscopy*; Oxford University Press: New York, 1986.
(62) Pollard, W. T.; Mathies, R. A. *Annu. Rev. Phys. Chem.* **1992**, *43*, 497.
(63) Levine, R. D.; Bernstein, B. R. *Molecular Reaction Dynamics and Chemical Reactivity*; Oxford University Press: New York, 1987.
(64) Martínez, T. J. *Chem. Phys. Lett.* **1997**, *272*, 139.